DNS of Couette flows with wall transpiration up to $Re_\tau = 1000$

S. Kraheberger

Chair of Fluid Dynamics
TU Darmstadt
Otto-Berndt-Str. 2, 64287 Darmstadt, Germany
kraheberger@fdy.tu-darmstadt.de

S. Hoyas

Instituto de Matemática Pura y Aplicada
Universitat Politècnica de València
Camino de Vera, 46024 València, Spain
sergio.hoyas@mot.upv.es

M. Oberlack

Chair of Fluid Dynamics
TU Darmstadt
Otto-Berndt-Str. 2, 64287 Darmstadt, Germany
oberlack@fdy.tu-darmstadt.de

ABSTRACT

We present a new set of direct numerical simulation data of a turbulent plane Couette flow with constant wall-normal transpiration velocity V_0, such that there is blowing on the lower side and suction on the upper. Hence, there is no net change in flux to preserve periodic boundary conditions in streamwise direction. Simulations were performed at $Re_\tau = 250, 500, 1000$ with varying transpiration rates in the range of $V_0^+ \approx 0.03$ to 0.085. Additionally, a classical Couette flow case at $Re_\tau = 1000$ is presented for comparison.

As a first key result we found a considerably extended logarithmic region of the mean velocity profile, with constant indicator function $\kappa = 0.77$ as transpiration increases. Further, turbulent intensities are observed to decrease with increasing transpiration rate. Mean velocities and intensities collapse only in the cases were the transpiration rate is kept constant while they are largely insensitive to friction Reynolds number variations. The long and wide characteristic stationary rolls of classical turbulent Couette flow are still present for all present DNS runs. The rolls are affected by wall transpiration, but they are not destroyed even for the largest transpiration velocity case. Spectral information indicate the prevalence of the rolls and the existence of wide structures near the blowing wall *http://www.fdy.tu-darmstadt.de/dns_database/direct_numerical_simulation.de.jsp* .

INTRODUCTION

Direct Numerical Simulation (DNS) is a fundamental tool for the study of wall turbulence, and it is the only available one when experiments are difficult, or simply impossible, to perform. Focusing on turbulent channel flow, there has been a continuous increase in Reynolds number of simulation of Poiseuille flows since the seminal work of Kim *et al.* (1987), followed by the works of Moser *et al.* (1999), Del Alamo *et al.* (2004), also Hoyas & Jiménez (2006) and, the very recent works by Bernardini *et al.* (2014) and Lee & Moser (2015). Turbulent Couette flows have been studied less, most probably due to the long and wide streamwise rolls existing in this flow, as it has been stated experimentally (Tillmark, 1995; Kitoh *et al.*, 2005; Kitoh & Umeki, 2008) and numerically (Bech *et al.*, 1995; Komminaho *et al.*, 1996; Tsukahara *et al.*, 2006; Pirozzoli *et al.*, 2011, 2014; Avsarkisov *et al.*, 2014*a*). The necessity of large boxes to capture these structures makes the study of this flow much more computationally expensive than a turbulent Poiseuille flow. Furthermore, these rolls seem to grow with Reynolds number, while at the same time the Kolmogorov scale decreases. In the case of non-canonical boundary conditions such as wall-normal transpiration, the bibliography for both type of channel flows is considerably reduced. For Poiseuille Transpiration Flow (PTF), the interest reader is referred to Avsarkisov *et al.* (2014*b*). In the case of a turbulent Couette with wall Transpiration Flow (CTF), up to the knowledge of the authors, the present study is the first work addressing this phenomenon. Moreover, the kinematics of CTF are more similar to turbulent asymptotic suction boundary layers (TASBL, see for instance Bobke *et al.* (2015) and references therein) than to PTF. This was somehow expected as in the TASBL, the thickness of the boundary layer is kept constant through the use of suction. An interesting conclusion of Bobke *et al.* (2015) is that realistic experiments of this kind of flows are nearly impossible.

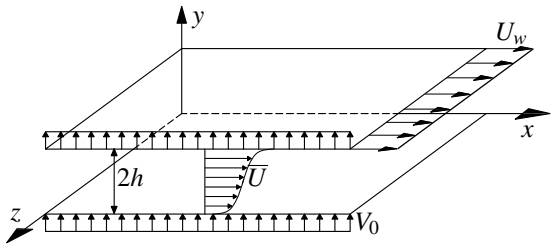

Figure 1: Schematic view of Couette flow with the moving wall velocity U_w and wall-normal transpiration velocity V_0. Fluid is blown through the lower wall and removed from the upper wall at a constant rate. The computational box is not scaled.

NUMERICAL METHOD

In this work, a new set of DNS of a plane CTF has been conducted within a computational box of $L_x = 8\pi h$, $L_y = 2h$ and $L_z = 3\pi h$, with spanwise and streamwise periodicity. In the past, this box has been used for very large turbulent Poiseuille flow simulations (Hoyas & Jiménez, 2006; Lee & Moser, 2015). However, it is known from the work by Avsarkisov *et al.* (2014*a*) that this computational box might be too narrow and short to adequately reproduce a turbulent Couette Flow. In the spanwise direction, it was confirmed in Pirozzoli *et al.* (2014), that for pure Couette flow the correlation length in this direction is nominally infinity. In the case of the streamwise correlation length, we are interested to investi-

Case	Line	Re_τ	Re_{V_0}	U_w/V_0	U_w/U_w^{C00}	V_0^+	N_x	N_y	N_z	TU_b/L_x	Tu_τ/h
C00	—○—	1000	0	∞	1	0	6144	383	4608	9.0	20.5
C02	·····	1000	32	1243	1.382	0.032	3072	383	2304	18.7	32.2
C05	– – – –	1000	50	685	1.907	0.051	3072	383	2304	22.0	60.1
C10	—·—	1000	60	492	2.741	0.063	3072	383	2304	22.0	97.5
C20	——	1000	75	395	4.402	0.071	3072	383	2304	24.7	194
A12	—▽—	250	19	400	2.673	0.070	768	251	576	60.6	281
A15	—△—	500	37.5	400	3.342	0.070	1536	251	1152	25.4	151
A20	—◇—	500	42	323	3.60	0.085	1536	251	1152	52.3	344

Table 1: Parameters of the simulations. Three different Reynolds numbers are presented: Re_τ is based on the mean friction velocity and the channel half-width h and Re_{V_0} is based on the transpiration velocity V_0 and h. The third column, U_w/V_0, is the ratio between the velocity of the wall U_w and V_0, which defines a Reynolds number usually employed for TASBL, see Bobke *et al.* (2015). Next, the velocities U_w and V_0 are given in terms of the wall-velocity of the pure Couette case, U_w^{C00}, and the mean friction velocity u_τ, respectively. N_x, N_y, N_z are the numbers of collocation points. The last two columns denote the computational time span while statistics were taken in wash-outs (U_b/L_x) and eddy turn-overs (u_τ/h). T is the computational time spanned by those fields. Line shapes given in the second column are used to identify the cases through all the figures of the present paper.

gate if the transpiration velocity is capable of breaking down the large streamwise rolls appearing in classical Couette Flows. Thus, the size of the box is a compromise between the capacity of running enough parametric cases and a large enough box to capture some of the largest scales of the flow.

The streamwise, wall-normal, and spanwise coordinates are x, y, and z and the corresponding velocity components are U, V and W or, using index notation, U_i. Statistically averaged quantities are denoted by an overbar, whereas fluctuating quantities are denoted by lowercase letters, i. e. $U = \overline{U} + u$. The flow is driven by a constant velocity of the upper wall such that we have the boundary condition $U(x,0,z) = 0$ and $U(x,2h,z) = U_w$. The blowing-suction process is implemented through the boundary condition $V(x,0,z) = V(x,2h,z) = V_0$, where V_0 is the constant transpiration velocity. The nominal Reynolds numbers studied are $Re_\tau = 250, 500$ and 1000, based on the mean friction velocity u_τ and on the channel half-width h. In all cases the mass flow is keep constant at 0.89, similar to Hoyas & Jiménez (2006); Avsarkisov *et al.* (2014*a*). The mean friction velocity is defined as $u_\tau = \sqrt{\frac{(u_\tau^b)^2 + (u_\tau^s)^2}{2}}$, where the local friction velocities are $u_\tau^b = \sqrt{\nu \left|\partial_y U\right|^b}$ and $u_\tau^s = \sqrt{\nu \left|\partial_y U\right|^s}$. Here and subsequently, superscripts b and s correspond to variables taken on the blowing and the suction side, respectively. See figure 1 for a sketch of the previously described boundary conditions.

The Navier-Stokes equations, employed to investigate the present flow, are discretized as described in Avsarkisov *et al.* (2014*b*). Initial fields were either taken from previously calculated Couette flows, imposing the new boundary conditions, or by increasing the transpiration velocities in previously computed cases.

Due to the lack of experimental data or numerical simulations, it has been impossible to do a formal validation of the code. However, in the past the code has been employed to successfully run simulations of turbulent Poiseuille flows (Hoyas & Jiménez, 2006; Hoyas & Jiménez, 2008), turbulent Couette flows (Avsarkisov *et al.*, 2014*a*) and turbulent PTF (Avsarkisov *et al.*, 2014*b*), while the modifications in the code to impose the new boundary condition have been minimal. In addition, simulations conducted at very low transpiration velocity were similar to pure Couette flows. A comparison with the laminar solution, which can be derived analytically in form of an exponential function, and a comparison with the first $Re_\tau = 1000$ simulation reported (Pirozzoli *et al.*, 2014) has been performed. Tests show a perfect agreement between DNS data and the analytic solution, though these results are omitted for brevity.

Table 1 summarizes the parameters of the present simulations. The wall-normal grid spacing is adjusted to keep the resolution at $\Delta y = 1.5\eta$, i. e., approximately constant in terms of the local isotropic Kolmogorov scale $\eta = (\nu^3/\varepsilon)^{1/4}$ for every Re_τ case. In wall units, Δy^+ varies from 0.42 at the wall up to $\Delta y^+ \simeq 7.2$ at the centerline. The wall-parallel resolution in Fourier Space for x and z is $\Delta x^+ \sim 12.2$ and $\Delta z^+ \sim 6.13$. The case C00 is a pure turbulent Couette flow in a $16\pi h \times 2h \times 6\pi h$ computational box used as a reference case. The transpiration velocity grows for the cases C02 to C20. Cases A15 and A12 were ran to study the effect of increasing Re_τ keeping the dimensionless parameters U_w/V_0 and V_0^+ approximately constant. Case A20 was employed to see the effects of a higher transpiration rate at a lower Reynolds number.

In every simulation, the flow had to evolve from an initial file, which has been taken from previous different simulations. The code was run until some transition phase has passed and the flow had adjusted to the new set of parameters. These transitions until the simulations reached a statistically steady state, which can be very time consuming, are not contemplated in the most right column of table 1. One of the measures used to asses that the code has run enough time to compile accurate statistics, is to compute the total shear stress, which for the CTF reads $\tau_b + V_0\bar{U} = \nu\frac{d\bar{U}}{dy} - \overline{uv}$, and, non-dimensionalized by u_τ^b, yields

$$1 + V_0^{+b}\bar{U}^{+b} - \frac{d\bar{U}^{+b}}{dy^{+b}} + \overline{uv}^{+b} = 0. \tag{1}$$

Another important consequence of this equation is that, evaluating it at the upper wall and employing the local friction velocities, we obtain

$$(u_\tau^s)^2 - (u_\tau^b)^2 = V_0 U_w, \tag{2}$$

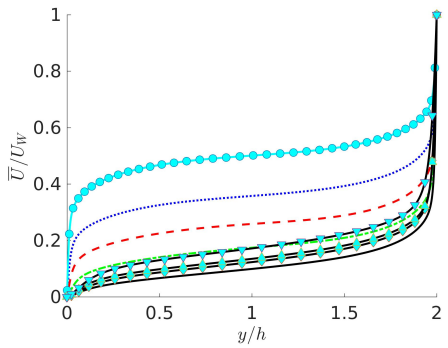

Figure 2: Lines as in Table 1. Mean velocity profile scaled in outer scales (U_w, h).

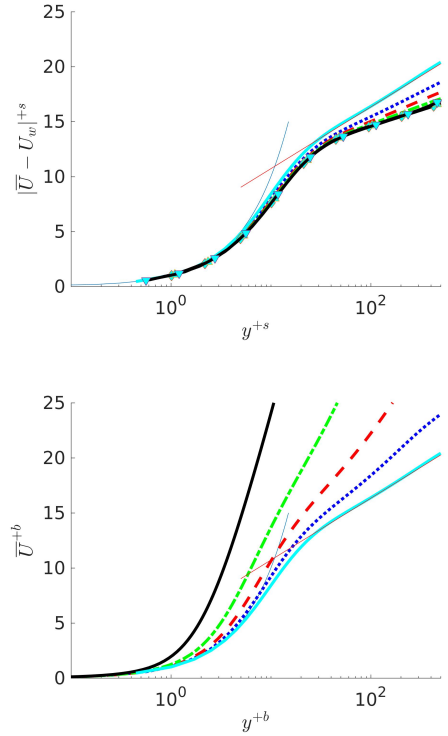

Figure 3: Lines as in Table 1. Mean velocity profile scaled in inner local scales at the suction (a) and blowing (b) sides. Blue thin solid line corresponds to viscous sublayer linear scaling law; red thin solid line represents near-wall classical logarithmic scaling law at $\kappa = 0.41$ and $B = 5$.

linking friction velocities with the value of the transpiration and the moving wall velocity.

In the present study we restrict ourselves to describe the new data coming from these simulations and to compare them with the results obtained for the pure Couette flow and other flows with wall transpiration and pointing out the key differences.

STATISTICS

Mean velocity profile

The mean velocity profiles may be taken from figure 2. This figure shows how transpiration leads to the loss of symmetry even for small V_0^+, leading to increasingly higher mean velocity gradients at the suction wall and lower gradients at the blowing wall.

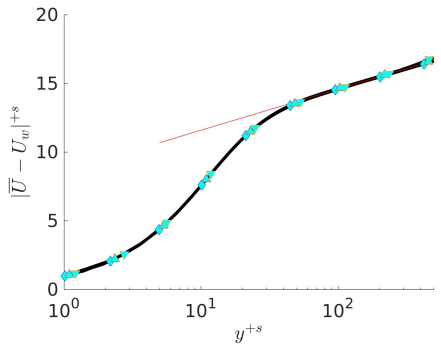

Figure 4: Lines as in Table 1. Mean velocity profile at the suction side scaled in u_τ^s. Cases plotted: C20, A12, A15 and A20. Red thin solid line represents modified logarithmic scaling law for $\kappa = 0.77$ and $B = 8.7$.

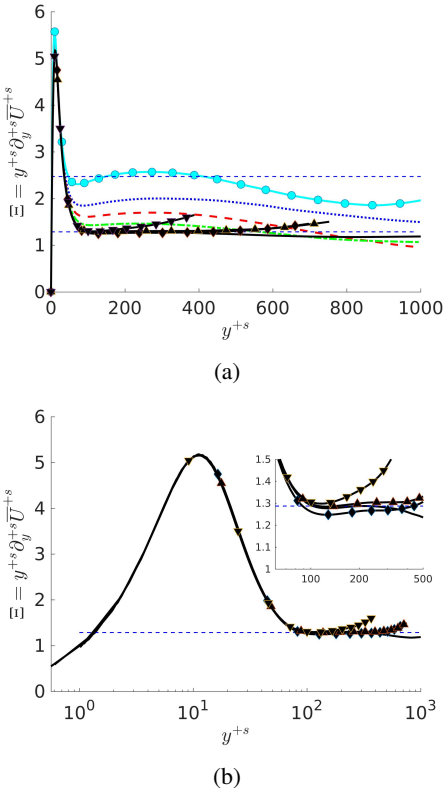

Figure 5: Lines as in Table 1. Indicator function for the logarithmic layer, i. e. the inverse of the von-Kármán-constant scaled with u_τ^s, (a) with dashed lines at $\kappa = 0.41$ and $\kappa = 0.77$, (b) in semi-logarithmic plot. Suction wall is at the left side of the plots.

Figure 3 shows $\overline{U}$ at the suction and blowing sides scaled by the local u_τ. At the suction wall the flow appears to follow the linear law in the viscous sublayer. However, at the blowing wall the interval where the linear law holds is shorter than the one near the suction side, and it gets further reduced as the transpiration number is increased. In the same figure, the red solid line shows the logarithmic profile, $\bar{U} = \frac{1}{\kappa}\ln y^+ + B$ at the classical coefficient values of $\kappa = 0.41$ and $B = 5.1$ Pope (2000). Qualitatively, the deviation from this logarithmic profile is in accordance with Sumitani &

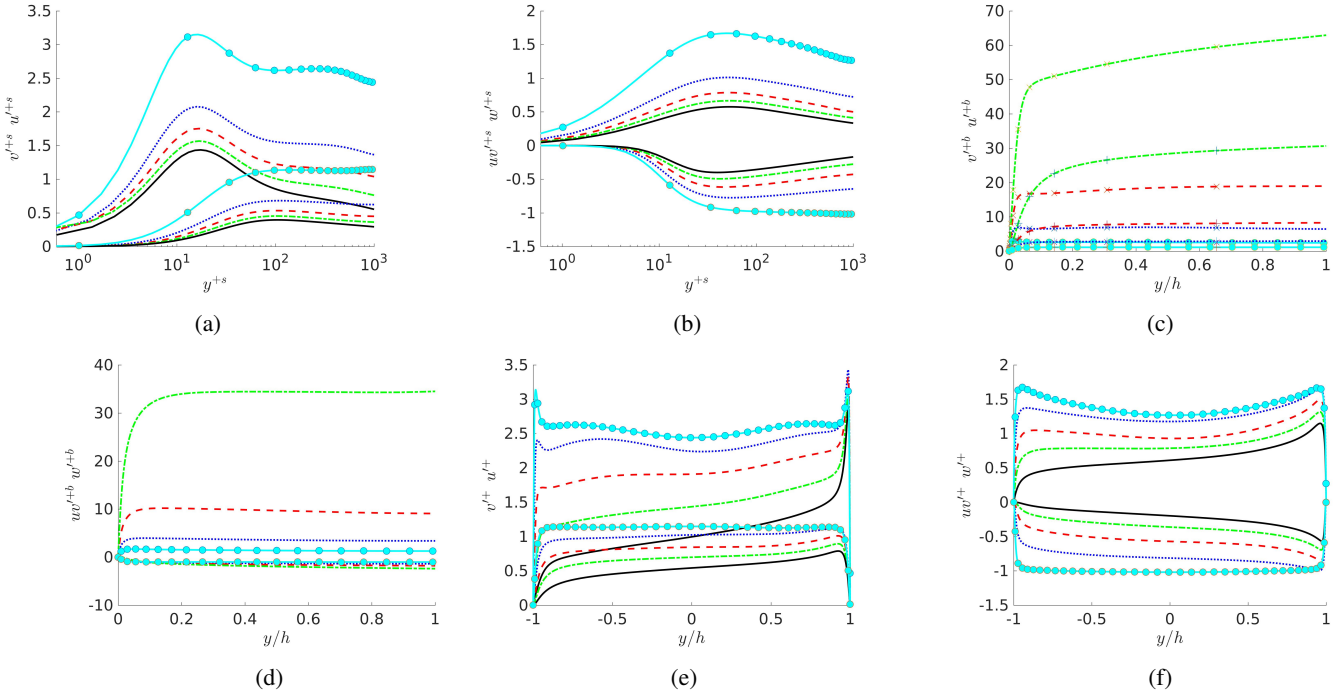

Figure 6: Lines as in Table 1. Velocity fluctuation intensities of the CXX-cases. Left column, u' and v'; right column w' and $\overline{uv}$. (a) and (b) adimensionalized by u_τ^s, plotted versus dimensionless distance from the suction wall in local inner units ($y_s^{+s} = (2-y/h)u_\tau^s/\nu$). (c) and (d) adimensionalized by u_τ^b, plotted versus distance from blowing wall in outer units. (e) and (f) adimensionalized by u_τ.

Kasagi (1995) and Kametani *et al.* (2015). This change in the slope seems to stop when V_0^+ is larger than 0.07 approximately, correspondig to $U_\infty/V_0 \leq 400$. Figure 4 shows $\overline{U}$ for the C20 and all A cases compared to a modified log law with $\kappa = 0.77$ and $B = 8.7$, with an excellent agreement.

However, using LES, Schlatter & Örlü (2011) gave a value of $\kappa = 0.82$ and $B = 9.2$ for a TASBL, independent of both U_∞/V_0 and Re_τ numbers. Further, Bobke *et al.* (2015) observed $\kappa = 0.89$ and $B = 9.6$ for a TASBL at $U_\infty/V_0 = 333$. It is clear from figure 3, that the slope of $\overline{U}$ changes with U_∞/V_0.

Figure 5 shows the mean velocity profile in terms of the inverse of the Kármán constant $\frac{1}{\kappa} = y^{+s}\partial U^{+s}/\partial y^{+s} = \Xi$, which is the definition of the log-indicator function. Apparently, with increasing transpiration rate, the region where this term is almost constant increases drastically. In fact, for the highest transpiration rate presented here, an approximately constant region between $y^{+s} = 80$ and $y^{+s} = 1000$ can be observed. This flattening effect is related to the vanishing of the secondary maximum that exists around 300^+ for the C00 case. The value of the log indicator function Ξ for the second set of simulations (C20, A20, A15 and A12) can be seen in the semi-logarithmic representation in figure 5b. There is a perfect collpase of the data below the logarithmic layer, i.e. essentially comprising the viscous sub-layer and the buffer layer, as the lower Reynolds number cases A collapse onto the $Re_\tau = 1000$ curve. All cases present a similar extended region, and in the range of traspiration numbers studied, this seems to be an intermediate limit. The existence of a displaced secondary maximum or minima can be discarded in the range of the presently studied parameters.

One of the possible reasons for the greatly extended range of validity of the log-region might be the value of u_τ^s which is ten times larger than the one for the classical Couette flow. As will be shown later, this effect can also be tentatively linked to the size and structure of the eddies present in the flow.

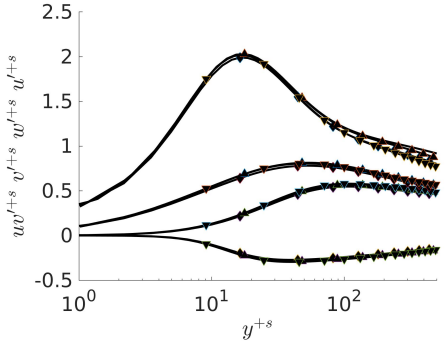

Figure 7: Lines as in Table 1. Velocity fluctuation intensities of the AXX and C20 cases plotted over dimensionless distance from the suction wall in local inner units

Turbulent intensities

In figure 6, the root-mean-square velocity fluctuations $u_i'^+ = \left(\overline{u_{[i]}u_{[i]}}^+\right)^{1/2}$, where index in brackets denote no summation, and $uv'^+ = \overline{uv}^+$ are presented for the different transpiration cases to be also compared to the pure Couette case. As for the mean velocity $\overline{U}$, the scaling with a local u_τ does not collapse the data.

It should be mentioned that normalization is not trivial here, since there are several velocity scales acting on the flow. Through the BC we have the external scales U_w and V_0, while internally we have the two friction velocities u_τ^s and u_τ^b, which are all related through the global momentum balance in equation 2. As was also observed in previous works investigating the TASBL, (Sumitani &

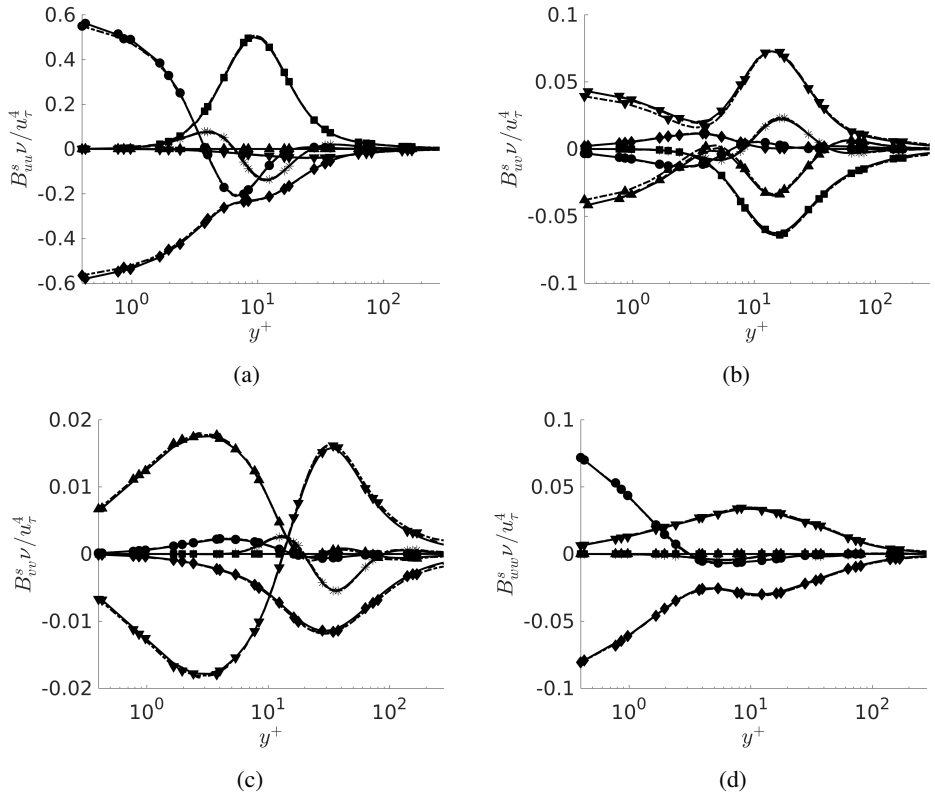

Figure 8: Budgets for Reynolds stresses. Cases for $V_0^+ = 0.07$ at the suction side are shown. (a) B_{uu}, (b) B_{uv}, (c) B_{ww}, (d) B_{ww}. Production $\square$, dissipation $\Diamond$, viscous diffusion $\circ$, pressure-strain $\triangledown$, pressure diffusion $\triangle$, turbulent diffusion $*$. Lines change from Table 1. Case C20, solid. Case A15, dashed. Case A12, dash-dot.

Kasagi, 1995; Kametani *et al.*, 2015; Schlatter & Örlü, 2011; Bobke *et al.*, 2015), we also find that scaling with the local friction velocity the turbulent intensities get reduced at the suction wall and increase near the blowing wall. Further, the known peaks of $u_i'^+$ and $w_i'^+$ (Hoyas & Jiménez, 2006; Avsarkisov *et al.*, 2014*b*) disappear at the blowing wall.

The situation when keeping the transpiration rate constant, while at the same time varying the Reynolds number, i. e. comparing the C20 case and all A cases is depicted in figure 7. In this case the local friction velocity u_τ^s seems to be the most appropriate scaling as it nicely collapses the data, but it fails completely in the suction wall (not shown). This failure is apparently a consequence of the term $V_0 U_w$ in the momentum conservation equation, as the product $U_w^+ V_0^+$ is constant for the C20 and A cases. This apparent scaling problem near the suction side will be studied in a companion paper. To facilitate the visualization and the comparison between both walls, in most of the figures and discussion that follows, global wall units will be used.

Turbulent budgets

The budget equation for the Reynolds-stress tensor components $\overline{u_i u_j}$, is given by

$$B_{ij} \equiv \frac{D\overline{u_i u_j}}{Dt} = P_{ij} + \varepsilon_{ij} + T_{ij} + \Pi_{ij}^s + \Pi_{ij}^d + V_{ij}, \tag{3}$$

where D/Dt is the mean substantial derivative and $(u_1, u_2, u_3) = (u, v, w)$. The different terms on the right hand side are referred to as production, dissipation, turbulent diffusion, pressure-strain, pressure diffusion, and viscous diffusion. They are respectively defined according to

$$P_{ij} = -\overline{u_i u_k}\partial_{x_k}\overline{U}_j - \overline{u_j u_k}\partial_{x_k}\overline{U}_i, \tag{4a}$$

$$\varepsilon_{ij} = -2\nu\overline{\partial_{x_k} u_i \partial_{x_k} u_j}, \tag{4b}$$

$$T_{ij} = -\partial_{x_k}\overline{u_i u_j u_k}, \tag{4c}$$

$$\Pi_{ij}^s = \overline{p(\partial_{x_j} u_i + \partial_{x_i} u_j)}, \tag{4d}$$

$$\Pi_{ij}^d = -\partial_{x_k}\left(\delta_{ki}\overline{p u_j} + \delta_{kj}\overline{p u_i}\right), \tag{4e}$$

$$V_{ij} = \nu\partial_{x_k}\partial_{x_k}\overline{u_i u_j}, \tag{4f}$$

In the previous definitions, δ_{ij} is Kronecker's delta and repeated index imply summation over $k = 1, 2, 3$. In canonical wall flows without wall-transpiration (Hoyas & Jiménez, 2008; Avsarkisov *et al.*, 2014*a*), $D\overline{u_i u_j}/Dt$ is zero. However, as soon as V_0 is different from zero, the convective derivative in y–direction does not vanish. Hence, from the four terms, the only remaining one is $B_{ij} = V_0\partial_{x_2}\overline{u_i u_j}$.

Selected non-trivial budgets are shown in figures 8, and, because of limited space, only some cases are plotted. The data from all the cases can be downloaded from our webpage given at the end of the abstract above. A general observation is that transpiration leads to a reduction of essentially all terms in the balance equation for $\overline{u_i u_j}$ in (3). Near the blowing wall, the values are several orders of magnitude smaller than at the suction wall (not shown). The peaks of the different quantities are in the same location as for the canonical flows Hoyas & Jiménez (2008). As it happens for the turbulent intensities, u_τ alone seems not sufficient to properly

scale i.e. collapse the turbulent budget. However, studying a constant suction at varying Reynolds number, i.e. considering the case of $V_0^+ = 0.07$, the curves of the budgets B_{uu} and B_{ww} for the cases A12, A15 and C20 collapse into one curve, as can be seen in figure 8. This clearly indicates that the value of V_0^+ is the key parameter for most of the turbulence properties.

The data presented in this section are in agreement with several other works of Sumitani & Kasagi (1995); Kametani *et al.* (2015); Bobke *et al.* (2015), when the local friction velocity is used for scaling the flow. The value of the intensities increase near the blowing wall and decrease close to the suction side as expected. However, this effect is larger than in the flows studied previously. At the blowing wall, as the transpiration velocity increases, the value of Re_τ^b gets reduced. For $V^+ > 0.06$ the known peaks of the intensities of $u_i'^{+b}$ and $w_i'^{+b}$ disappear. As a difference to previous works, the global Re_τ can be used to analyze the behavior of the flow at both walls. The damping of turbulence induced by the reduction of the local friction velocity at the blowing wall, does not coincide with an increase of the turbulent budgets near the blowing wall when $V^+ > 0.06$ as turbulence is dampened in both walls, when scaled in global wall units.

CONCLUSION

We have presented, for the first time, a set of turbulent plane Couette flow simulations extended by a wall-normal transpiration velocity. The main importance of the present paper lies in the investigation of the effects due to the transpiration velocity and the analysis of the turbulent structures detected in the flow which are rather distinct on the blowing side and the suction side. A second important point is the search for the proper velocity scales to appropriately scale the flow and collapse the statistical data. The main difficulty about the latter issue is due to the four velocities acting on the flow. In particular, we have the external velocities U_w and V_0 extended by the two local friction velocities u_τ^s and u_τ^b, although they are all interconnected by the mean momentum equation (1).

From the computations at the highest transpiration number, i. e., $V_0^+ = 0.07$, we observe a collapse of the mean velocity and the second moments in wall units for different Reynolds numbers, essentially showing that V_0^+ is the key parameter to control the flow acting as an invariant. This number has been previously used as Reynolds number in TASBL with injection and suction. Further, it is observed that at the highest Reynolds number and the highest transpiration rate, the slope constant of the logarithmic law increases to $\kappa = 0.77$ representing an extremely extended logarithmic region, much longer than the one that can be observed in turbulent Poiseuille or Couette flows at similar Reynolds numbers. Further, one of the main effects of transpiration is the reduction of the value of turbulent intensities and $\overline{uv}^+$, and thus a general reduction of turbulence in the flow.

It is noteworthy to mention that the long and wide structures characteristic of turbulent Couette flows at zero transpiration, are still present. Their footprints are still present in the one-dimensional spectra of the flow. The only small change is that this structures are moved towards the suction wall. The spectra near the blowing wall presents two peaks, created by the transmission of energy due to the transpiration velocity.

REFERENCES

Avsarkisov, V., Hoyas, S., Oberlack, M. & García-Galache, J.P. 2014*a* Turbulent plane Couette flow at moderately high reynolds number. *Journal of Fluid Mechanics* **751**, R1.

Avsarkisov, V., Oberlack, M. & Hoyas, S. 2014*b* New scaling laws for turbulent Poiseuille flow with wall transpiration. *Journal of Fluid Mechanics* **746**, 99–122.

Bech, K., Tillmark, N., Alfredsson, P. & Andersson, H. 1995 An investigation of turbulent plane Couette flow at low Reynolds numbers. *Journal of Fluid Mechanics* **286**, 291325.

Bernardini, M., Pirozzoli, S. & Orlandi, P. 2014 Velocity statistics in turbulent channel flow up to $Re_\tau = 4000$. *Journal of Fluid Mechanics* **758**, 327343.

Bobke, A., Örlü, R. & Schlatter, P. 2015 Simulations of turbulent asymptotic suction boundary layers. *Journal of Turbulence* **17** (2), 157–180.

Del Alamo, J.C., Jiménez, J., Zandonade, P. & Moser, R.D. 2004 Scaling of the energy spectra of turbulent channels. *Journal of Fluid Mechanics* **500**, 135144.

Hoyas, S. & Jiménez, J. 2006 Scaling of the velocity fluctuations in turbulent channels up to $Re_\tau = 2003$. *Physics of Fluids (1994-present)* **18** (1), 011702.

Hoyas, S. & Jiménez, J. 2008 Reynolds number effects on the Reynolds-stress budgets in turbulent channels. *Physics of Fluids* **20** (10), 101511.

Kametani, Y., Fukagata, K., Örlü, R. & Schlatter, P. 2015 Effect of uniform blowing suction in a turbulent boundary layer at moderate reynolds number. *International Journal of Heat and Fluid Flow* **55**, 132–142.

Kim, J., Moin, P. & Moser, R. 1987 Turbulence statistics in fully developed channels flows at low Reynolds numbers. *Journal of Fluid Mechanics* **320**, 259–285.

Kitoh, O., Nakabyashi, K. & Nishimura, F. 2005 Experimental study on mean velocity and turbulence characteristics of plane Couette flow: Low-Reynolds-number effects and large longitudinal vortical structure. *Journal of Fluid Mechanics* **539**, 199–227.

Kitoh, O. & Umeki, M. 2008 Experimental study on large-scale streak structure in the core region of turbulent plane Couette flow. *Physics of Fluids* **20** (2), 025107.

Komminaho, J., Lundbladh, A. & Johansson, A. 1996 Very large structures in plane turbulent Couette flow. *Journal of Fluid Mechanics* **320**, 259–258.

Lee, M. & Moser, R. 2015 Direct numerical simulation of turbulent channel flow up to $Re_\tau \approx 5200$. *Journal of Fluid Mechanics* **774** (395-415).

Moser, R.D., Kim, J. & Mansour, N.N. 1999 Direct numerical simulation of turbulent channel flow up to $Re_\tau = 590$. *Physics of Fluids* **11** (4), 943–945.

Pirozzoli, S., Bernardini, M. & Orlandi, P. 2011 Large-scale motions and inner/outer layer interactions in turbulent Couette-Poiseuille flows. *Journal of Fluid Mechanics* **680**, 534–563.

Pirozzoli, S., Bernardini, M. & Orlandi, P. 2014 Turbulence statistics in couette flow at high reynolds number. *Journal of Fluid Mechanics* **758** (323-343).

Pope, S. B. 2000 *Turbulent flows*. Cambridge University Press.

Schlatter, P. & Örlü, Ramis 2011 Turbulent asymptotic suction boundary layers studied by simulation. *Journal of Physics: Conference Series* **318**, 022020.

Sumitani, Y. & Kasagi, N. 1995 Direct numerical simulation of turbulent transport with uniform wall injection and suction. *AIAA Journal* **33**, 1220–1228.

Tillmark, N. 1995 Experiments on transition and turbulence in plane Couette flow. PhD thesis, KTH, Royal Institute of Technology.

Tsukahara, T., Kawamura, H. & Shingai, K. 2006 DNS of turbulent Couette flow with emphasis on the large-scale structure in the core region. *Journal of Turbulence* **7**, 1–16.